Prediction of ^{195}Pt NMR Chemical Shifts by Density Functional Theory Computations: The Importance of Magnetic Coupling and Relativistic Effects in Explaining Trends

Thomas M. Gilbert*,[1] and Tom Ziegler*

Department of Chemistry, University of Calgary, 2500 University Drive NW, Calgary, Alberta, Canada T2N 1N4

Received: June 29, 1999

Density functional theory with relativistic corrections has been used to calculate the ^{195}Pt chemical shifts for a series of Pt(II) complexes. Good agreement with experimental values is observed with two different relativistic correction methods. Deconvolution of the parameters leading to the overall shielding of the platinum nucleus shows that both the paramagnetic and the spin−orbit shielding terms contribute substantially. Detailed transition analysis demonstrates that the most important contributions to the paramagnetic shielding for PtX_4^{2-} anions and *cis*- and *trans*-$PtX_2(NH_3)_2$ compounds come from the Pt d_{xy}−X lone pair $\pi \rightarrow$ Pt $d_{x^2-y^2}$−X σ^* and Pt d_{xy}−X lone pair $\pi^* \rightarrow$ Pt $d_{x^2-y^2}$−X σ^* transitions, in accord with qualitative predictions. For *cis*- and *trans*-PtX_2L_2 complexes (L = PMe_3, $AsMe_3$, SMe_2), the Pt d_{xy}−X lone pair $\pi \rightarrow$ Pt $d_{x^2-y^2}$−X σ^* transition is most important, but the Pt d_{xy}−X lone pair $\pi^* \rightarrow$ Pt $d_{x^2-y^2}$−X σ^* transition is much less so. This is readily understood through recognition of the importance of the magnetic coupling term to the paramagnetic shielding. The trend that chemical shifts vary as $I^- < Br^- < Cl^-$ arises from the magnetic coupling term and the spin−orbit contribution; it runs counter to the trend predicted by the energy gaps between the orbitals involved in the important transitions.

Introduction

Experimental NMR studies of the ^{195}Pt nucleus are numerous, owing to its favorable observation characteristics and to the importance of platinum compounds as archetypes of square-planar species, as antitumor agents, and as catalysts.[2] Theoretical rationalization and prediction of ^{195}Pt NMR chemical shifts dates to the late 1960s, when Pidcock et al.[3] and Dean and Green[4] (PDG) applied Ramsey's equation for paramagnetic shielding to square-planar D_{4h} PtX_4^{2-} systems. Dean and Green used their expression and visible absorption and ^{195}Pt NMR data for a series of *trans*-$Pt(PEt_3)_2HL$ compounds to argue that the covalency of the platinum−ligand bonds contributed more to the platinum chemical shift than did orbital energy gaps. Later, Goggin et al.[5] employed the PDG equation and a fitting procedure to provide relative covalencies for the ligands in a series of PtX_3L^- anions, finding that larger, softer ligands formed more covalent interactions with the soft Pt(II) center than smaller, harder ligands, in keeping with hard−soft acid−base (HSAB) theory. Appleton et al.[6] similarly rationalized the shifts in several pseudo-square-planar Pt(II) systems.

Considering this promising theoretical start, surprisingly little detailed computational work on ^{195}Pt NMR shifts has appeared. This certainly reflects the difficulty in calculating systems containing so many electrons. Extended Hückel (EHMO) methods were used to predict shifts in some Pt (0) acetylene complexes,[7] but the technique was not extended. This lack is unfortunate, because accurate prediction of Pt(II) NMR shifts would find use in the fields noted above.

A further motivation for examining ^{195}Pt NMR chemical shifts theoretically is the opportunity given to study the importance of relativistic effects on them. Recent work has demonstrated the importance of including such effects when predicting the ^{13}C NMR shifts in compounds such as CHI_3 and CI_4,[8] and the ^{199}Hg shifts in any mercury compounds.[9] Different means have appeared to incorporate relativistic effects into calculations, with varying degrees of success.[10]

Our group has made considerable use of density functional theory (DFT) augmented by relativistic corrections to calculate NMR shifts of heavy atoms in compounds.[9a,10−12] Good agreement has generally been observed between calculated and experimental shifts, with the zeroth order regular approximation (ZORA) relativistic correction typically giving the best results. However, the work has shown that different shielding terms determine the chemical shift for different metals. For ^{183}W in $WX_nY_{4-n}^{2-}$ ions (X, Y = O, S),[12] the paramagnetic shift δ^p largely determines the chemical shift, as is common and expected. However, for ^{199}Hg in linear HgX_2 (X = halide, Me, SiH_3) compounds[9a] and ^{207}Pb in several Pb(II) and Pb(IV) compounds,[12a] the shift depends on both δ^p and the spin−orbit (relativistic) shift δ^{SO}. It is thus of interest to characterize the important factors for ^{195}Pt. If the relativistic spin−orbit shift is important, this could explain deviations between the PDG concept and experiment.

We report here calculations predicting the ^{195}Pt chemical shift for a series of square-planar Pt(II) compounds. Two types of relativistic correction were examined, the Pauli method and the ZORA method. A transition analysis confirms the utility of the PDG equation while revealing some of its limitations. The principal finding is that explaining several experimental trends in the chemical shift requires knowing the magnitudes of the energies of important electronic transitions, the magnetic coupling between the orbitals involved, and the relativistic spin−orbit contribution.

Computational Details, Methods, and Concepts

All DFT calculations were carried out using the Amsterdam Density Functional (ADF 2.3.3) program.[13] The functionals

10.1021/jp992202r CCC: $18.00
Published on Web 08/31/1999

employed included the local density approximation of Vosko, Wilk, and Nusair (LDA VWN)[14] augmented with the nonlocal gradient correction PW91 from Perdew and Wang.[15] Relativistic corrections were added using either a Pauli spin−orbit Hamiltonian[16] or the ZORA (zeroth order regular approximation) spin−orbit Hamiltonian.[9a]

Pauli calculations used the ZORA (IV) basis sets available in ADF; these mimic the standard ADF (IV) basis functions in that they span each shell with a set of triple-ζ Slater-type atomic orbitals and contain polarization functions for H−Ar and Ga−Kr. The basis functions were modified as described by van Lenthe.[17] Non-hydrogen atoms were assigned a relativistic frozen core potential, treating as core the shells up to and including 4f for Pt, 4p for I, 3p for Br and As, 2p for Cl, S, and P, and 1s for N and C. (Pauli calculations can only be carried out using the frozen core approximation due to variational instability of the Hamiltonian).[11a] Electrons in the core shells were represented by orbitals generated from atomic ZORA calculations and kept frozen.

We also performed quasirelativistic scalar Pauli calculations to provide purely real molecular orbitals and energies for the transition analysis. Visualization was accomplished through use of the program Viewkel.[18]

ZORA calculations employed the ZORA (IV) basis sets for Pt and atoms bound to it but used the ZORA (II) basis functions (double-ζ quality, without polarization) for peripheral carbon and hydrogen atoms. This allowed efficient calculation of the larger molecules. Examination of a few compounds in the data set suggested that the calculated ^{195}Pt shielding changed only slightly (ca. 50 ppm) when these simplified functions were used. In one set of calculations (ZORA core), the atoms were given frozen core potentials as above (the Pt basis set was not modified); in a second set (ZORA all), all electrons of Pt were treated as valence electrons, with frozen cores still assigned to the other atoms.

^{195}Pt NMR shieldings were calculated by the NMR program of Wolff et al.[9a,19] using the orbitals generated by the single-point run. The ^{195}Pt chemical shifts derived from the shielding values exhibited similar root-mean-square (rms) differences from the experimental values (Pauli, 315 ppm; ZORA core, 390 ppm; ZORA all, 336 ppm).

Metrical data were determined from examination of crystal structure data of several PtX_4^{2-} salts (X = Cl^-, Br^-, I^-), *cis*- and *trans*-$PtCl_2(NH_3)_2$, and a number of *cis*- and *trans*-$PtX_2(ZR_n)_2$ compounds (X = halide; Z = P, n = 3; Z = As, n = 3; Z = S, n = 2; R = alkyl group).[20] The Pt−X and Pt−Z bond lengths and the various angles around Pt of each type of compound/anion were averaged to provide reference values. These appear in Table 1. Studies of the relationship between the calculated ^{195}Pt NMR shift and the Pt−X and Pt−Z bond distances for several of the $PtX_2(ZMe_n)_2$ compounds revealed that the shifts varied by no more than 50 ppm/0.01 Å (see Supporting Information); so even if the values in Table 1 are somewhat in error, the shifts should not change drastically. The Pt and the four atoms bound to it were fixed to be coplanar. N−H and Z−C bond lengths were taken from compilations of crystal structure data.[21] C−Z−Pt and H−N−Pt angles were set to 109.5°. Examination of a number of different choices for dihedral angles for methyl carbons or ammonia hydrogens with respect to the central plane demonstrated that the calculated ^{195}Pt shift varied by less than 50 ppm over this "rotation". Methyl groups were given C−H bond distances of 1.10 Å, H−C−H angles of 109.5°, and torsion angles designed to minimize steric interactions.

TABLE 1: Distances (Å) and Angles (Deg) Used in the Calculations

	Pt−X	Pt−Z	X−Pt−X	Z−Pt−Z	other
$PtCl_4^{2-}$	2.31		90		
$PtBr_4^{2-}$	2.43		90		
PtI_4^{2-}	2.61		90		
cis-$PtCl_2(SMe_2)_2$	2.31	2.27	90	92	S−C 1.80
trans-$PtCl_2(SMe_2)_2$	2.30	2.30	90	90	
cis-$PtBr_2(SMe_2)_2$	2.43	2.27	90	92	
trans-$PtBr_2(SMe_2)_2$	2.42	2.30	90	90	
cis-$PtI_2(SMe_2)_2$	2.62	2.27	90	92	
trans-$PtI_2(SMe_2)_2$	2.61	2.30	90	90	
cis-$PtCl_2(NH_3)_2$	2.32	2.05	90	90	N−H 1.01
trans-$PtCl_2(NH_3)_2$	2.32	2.05	90	90	
cis-$PtBr_2(NH_3)_2$	2.43	2.05	90	90	
trans-$PtBr_2(NH_3)_2$	2.43	2.05	90	90	
cis-$PtI_2(NH_3)_2$	2.61	2.05	90	90	
trans-$PtI_2(NH_3)_2$	2.61	2.05	90	90	
cis-$PtCl_2(PMe_3)_2$	2.36	2.25	88	96	P−C 1.82
trans-$PtCl_2(PMe_3)_2$	2.31	2.31	90	90	
cis-$PtBr_2(PMe_3)_2$	2.48	2.25	88	96	
trans-$PtBr_2(PMe_3)_2$	2.43	2.31	90	90	
cis-$PtI_2(PMe_3)_2$	2.67	2.25	88	96	
trans-$PtI_2(PMe_3)_2$	2.61	2.31	90	90	
cis-$PtCl_2(AsMe_3)_2$	2.36	2.33	88	96	As−C 1.94
trans-$PtCl_2(AsMe_3)_2$	2.31	2.39	90	90	
cis-$PtBr_2(AsMe_3)_2$	2.48	2.33	88	96	
trans-$PtBr_2(AsMe_3)_2$	2.43	2.39	90	90	
cis-$PtI_2(AsMe_3)_2$	2.67	2.33	88	96	
trans-$PtI_2(AsMe_3)_2$	2.61	2.39	90	90	

Shielding. The total NMR shielding tensor σ for nucleus N contains paramagnetic, diamagnetic, and relativistic spin−orbit contributions, evaluated as

$$\sigma_{us} = \sigma_{us}^{d} + \sigma_{us}^{p} + \sigma_{us}^{SO} = \int \frac{\vec{r}_N \times [\vec{J}_s^{d}(\vec{r}_N) + \vec{J}_s^{p}(\vec{r}_N)]_u}{r_N^{3}} \, d\vec{r}_N + \sigma_{us}^{SO} \quad (1)$$

Here $\vec{J}^{d}$ and $\vec{r}J^{p}$ are respectively the diamagnetic and paramagnetic current densities induced by an external magnetic field $\vec{B}_o$ with components $\vec{B}_{o,s}$. Equation 1 involves an expectation value of r_N^{-3}, where r_N equals the distance between the NMR nucleus and the reference electron. The paramagnetic current density originates primarily from a coupling between occupied, Ψ_i, and virtual orbitals, Ψ_a, induced by the external magnetic field:

$$\vec{J}^{p} = \sum_{s=1}^{3} \vec{J}_s^{p} B_{o,s} = \sum_{s=1}^{3} \sum_{i}^{occ} \sum_{a}^{vir} \left(\frac{1}{c}\right) [u_{ai}^{(l,s)}][\Psi_i \nabla \vec{\Psi}_a - \Psi_a \nabla \vec{\Psi}_i] B_{o,s} \quad (2)$$

where c is the speed of light.

The principal contribution to the paramagnetic coupling $u_{ai}^{(l,s)}$ is given by

$$u_{ai}^{(l,s)} \overset{\propto}{\approx} -\frac{1}{2c(E_i^{(0)} - E_a^{(0)})} \sum_{\lambda,\nu} c_{\lambda a}^{(0)} c_{\nu i}^{(0)} \{\langle \chi_\lambda | [\vec{r}_\nu \times \bar{\nabla}]_s | \chi_\nu \rangle\} \propto -\frac{1}{2c(E_i^{(0)} - E_a^{(0)})} \langle \Psi_a | \hat{M}_s | \Psi_i \rangle \quad (3)$$

Here $E^{(0)}$ refers to orbital energies of the unperturbed molecule without the external magnetic field generated from a ZORA or Pauli calculation. $\langle \Psi_a | \hat{M}_s | \Psi_i \rangle$ represents the first-order magnetic coupling between an occupied and a virtual molecular orbital. Within the gauge-independent atomic orbital (GIAO) formalism

we use, the action of the magnetic operator $\hat{M}_s$ on Ψ_q is simply to work with $i\hat{L}_s^{\nu}$ on each atomic orbital x_ν. Here $\hat{L}_s^{\nu}$ equals the s-component of the angular momentum operator with its origin at the center $\vec{R}_\nu$ on which x_ν is situated. Tabulations for $\hat{L}_s^{\nu}x_\nu$ are available in the literature.[22,23]

We digress here to note the relationship between eqs 1−3 and the PDG eq 4:

$$\sigma^p = -K \times \langle r^{-3} \rangle \times \{C^2_{A_{1g}}[2C^2_{A_{2g}}(E_{^1A_{2g}} - E_{^1A_{1g}})^{-1} + C^2_{E_g}(E_{^1E_g} - E_{^1A_{1g}})^{-1}]\} \quad (4)$$

To reach this expression, PDG neglected first the ligand contributions to the magnetic moment $\langle \Psi_a|\hat{M}_s|\Psi_i\rangle$ in eq 3 so that only atomic orbital (AO) expansion coefficients C for the platinum d orbitals were retained in Ψ_a and Ψ_i. Further, in the same equation, the sum over transitions (i → a) was limited to two, the $^1A_{1g}$ (ground state) → $^1A_{2g}$ (excited state) and $^1A_{1g}$ → ^1E_g ones (see Results and Discussion section). Substituting the approximate expression for $u_{ai}^{(l,s)}$ into eq 1 and retaining again only platinum d-orbital contributions in Ψ_a and Ψ_i affords the PDG equation. PDG interpreted the C terms as describing the covalency of the ligand−metal interactions, where C values of 0.5 would correspond to covalent bonds, whereas C values of 1.0 or zero would indicate ionic bonds. Finally, the $\langle r^{-3}\rangle$ term in eq 4 matches that in the integral term of eq 1 except that $\langle r^{-3}\rangle$ is with respect to the radial part of the platinum d orbital.

In essence, one can think of the PDG equation as a submethod of our computational model. The model avoids the limitations imposed on eq 4, thereby providing a more realistic prediction of the chemical shift. As we shall see below; however, the two methods provide similar ways of visualizing why trends in ^{195}Pt chemical shift are as they are. Covalency in the PDG equation translates to the extent of magnetic coupling in our model.

The spin−orbit contribution to the shielding, σ_{us}^{SO}, is dominated by the Fermi-contact term:[19]

$$\sigma_{us}^{SO} = \sigma_{us}^{FC} = \frac{4\pi g}{3c}\sum_{i}^{occ}\sum_{a}^{vir} u_{ia}^{(l,s)}\langle \Psi_a|\hat{S}_u\delta(r_N = 0)|\Psi_i\rangle \quad (5)$$

where $\hat{S}_u$ is a Cartesian component of the electronic spin operator and g is the electronic Zeeman g-factor.

Chemical Shift. The calculated chemical shift equals the difference between the shielding of the reference and the shielding of the molecule of interest:

$$\delta = \sigma_{ref} - \sigma \quad (6)$$

Experimentally, the reference is Na_2PtCl_6 in water. To avoid experimental data taken in highly polar, coordinating solvents, we chose *cis*-$PtCl_2(SMe_2)_2$ as the reference.[5]

Combining eqs 1 and 6 gives the principle used in Table 2,

$$\delta(^{195}\text{Pt}) = \delta^d + \delta^p + \delta^{SO} \quad (7)$$

Results and Discussion

We selected the neutral *cis*- and *trans*-PtX_2L_2 compounds listed in Table 2 for examination because their experimental ^{195}Pt NMR chemical shifts were determined in relatively nonpolar, noncoordinating solvents,[5] and thus should be properly predicted by a "gas-phase" calculation. The experimental shifts are referenced to that of *cis*-$PtCl_2(SMe_2)_2$. Even though the compounds are structurally similar, the chemical shifts cover a range of ca. 3400 ppm (about 60% of the range of ^{195}Pt(II) shifts, about 25% of the range for all ^{195}Pt shifts)[2] and so provide a good test set for determining whether the computational method works.

TABLE 2: Calculated ^{195}Pt Chemical Shift Terms vs Experimental Shifts, in ppm[2,6 a]

compound	δ^p	δ^d	δ^{SO}	δ_{calc}	δ_{expt}	Δ
cis-$PtCl_2(SMe_2)_2$	0	0	0	0	0	
	[0]	[0]	[0]	[0]		
trans-$PtCl_2(SMe_2)_2$	64	10	−75	−1	127	128
	[94]	[−1]	[−87]	[6]		[121]
cis-$PtBr_2(SMe_2)_2$	−140	3	−247	−384	−328	56
	[−174]	[0]	[−183]	[−357]		[29]
trans-$PtBr_2(SMe_2)_2$	−245	12	−303	−536	−348	188
	[−262]	[0]	[−211]	[−473]		[125]
cis-$PtI_2(SMe_2)_2$	−421	−5	−716	−1142		
	[−797]	[−8]	[−472]	[−1277]		
trans-$PtI_2(SMe_2)_2$	−849	5	−793	−1637	−1601	36
	[−1288]	[−7]	[−430]	[−1725]		[124]
cis-$PtCl_2(NH_3)_2$	1485	11	−146	1350	1447	97
	[1710]	[0]	[−335]	[1375]		[72]
trans-$PtCl_2(NH_3)_2$	1177	13	−110	1080	1450	370
	[1506]	[1]	[−220]	[1287]		[163]
cis-$PtBr_2(NH_3)_2$	1220	14	−422	812	1092	280
	[1424]	[1]	[−497]	[928]		[164]
trans-$PtBr_2(NH_3)_2$	830	15	−306	539		
	[1169]	[2]	[−342]	[829]		
cis-$PtI_2(NH_3)_2$	676	6	−1008	−326	283	609
	[468]	[−8]	[−710]	[−250]		[533]
trans-$PtI_2(NH_3)_2$	165	8	−810	−637		
	[114]	[−5]	[−404]	[−295]		
cis-$PtCl_2(PMe_3)_2$	−522	17	234	−271	−857	−586
	[−331]	[3]	[177]	[−151]		[−706]
trans-$PtCl_2(PMe_3)_2$	−434	18	−72	−488	−399	89
	[−309]	[7]	[68]	[−234]		[−165]
cis-$PtBr_2(PMe_3)_2$	−582	20	43	−519	−1085	−566
	[−448]	[5]	[14]	[−429]		[−656]
trans-$PtBr_2(PMe_3)_2$	−736	20	−264	−980	−922	58
	[−636]	[8]	[−74]	[−702]		[−220]
cis-$PtI_2(PMe_3)_2$	−706	11	−284	−979	−1037	−58
	[−690]	[−6]	[−165]	[−861]		[−176]
trans-$PtI_2(PMe_3)_2$	−1285	13	−701	−1973	−1988	−15
	[−1418]	[1]	[−258]	[−1675]		[−313]
cis-$PtCl_2(AsMe_3)_2$	−391	12	163	−216	−740	−524
	[−250]	[1]	[33]	[−216]		[−524]
trans-$PtCl_2(AsMe_3)_2$	−313	13	1	−299	−229	70
	[−112]	[2]	[−39]	[−149]		[−80]
cis-$PtBr_2(AsMe_3)_2$	−498	15	−62	−545	−1074	−529
	[−405]	[3]	[−123]	[−525]		[−549]
trans-$PtBr_2(AsMe_3)_2$	−628	16	−225	−837	−827	10
	[−467]	[3]	[−183]	[−647]		[−180]
cis-$PtI_2(AsMe_3)_2$	−710	7	−489	−1192		
	[−783]	[−7]	[−426]	[−1216]		
trans-$PtI_2(AsMe_3)_2$	−1290	8	−701	−1983	−1967	16
	[−1412]	[−4]	[−439]	[−1855]		[−106]
RMS difference						315
						[330]

[a] Values calculated using the Pauli method (see text) are on top, those calculated using the ZORA all method are in brackets. δ^p,δ^d, and δ^{SO} are the paramagnetic, diamagnetic, and spin−orbit shifts, respectively. δ_{calc} and δ_{expt} are respectively the total calculated and experimental ^{195}Pt chemical shifts, referenced to *cis*-$PtCl_2(SMe_2)_2$. $\Delta = \delta_{expt} - \delta_{calc}$.

As noted in the Computational Details, Methods, and Concepts section, the three spin−orbit-corrected computational methods gave similar rms differences from experiment (ca. 300 ppm, approximately 10% of the chemical shift range). We show the data from the spin−orbit Pauli and the ZORA all electron calculations in Table 2. The overall shifts and Δ values for each method are similar. The ZORA frozen core values fell generally within 10−20% of the values of the all-electron ZORA method; this indicates that employing the frozen core approximation does not drastically affect the results.

The agreement between calculated and experimental values is generally good, in some cases excellent. Much of the rms difference arises from *cis*-$PtCl_2(PMe_3)_2$ and its bromide homologue, and *cis*-$PtCl_2(AsMe_3)_2$ and its bromide homologue. If one removes these compounds from the data set, the rms difference is more than halved. The root of the large errors lies in the fact that, regardless of the halide, the donor ligand, or the relativistic Hamiltonian employed, the computational model nearly always predicts cis compounds to exhibit more positive (higher frequency) shifts than the corresponding trans compounds, while experimentally, the four cis compounds noted display lower frequency, more negative shifts than do the trans isomers. Several possibilities exist to explain this dichotomy. We may have made poor choices for molecular metrical parameters for cis isomers, although our studies of the relationship between shielding and bond distance (see above) argue against this. Our method may simply do a poorer job generally of modeling cis compounds compared to trans compounds for some unknown reason; support for this arises from the fact that the agreement for *cis*-$PtI_2(NH_3)_2$ is also poor. Possibly the experimental values, which were determined by indirect resonance methods rather than by direct observation, are inaccurate. Perhaps a solvent effect which affects cis compounds more than trans compounds exists, which the model cannot take into account.

The calculations do model another experimental trend properly. It is well-known that substituting a softer ligand for a harder one causes the ^{195}Pt resonance to shift to more negative values.[2] One sees this in two ways in Table 2. First, as the halide of a set of PtX_2L_2 molecules becomes heavier and thus softer, (Cl < Br < I), $\delta(^{195}Pt)$ becomes more negative. This arises because both the paramagnetic shift δ^p and the spin−orbit shift δ^{SO} concomitantly become more negative down the halide family. Second, as the ligand L becomes softer, the ^{195}Pt resonance again shifts to lower frequency. For example, $PtX_2(NH_3)_2$ species exhibit shifts much more positive than those of the corresponding $PtX_2(PMe_3)_2$ species. The same trend is largely, though not entirely observed when one compares $PtX_2(PMe_3)_2$ compounds with $PtX_2(AsMe_3)_2$ compounds; this presumably reflects the similar "softnesses" of the PMe_3 and $AsMe_3$ ligands.

The data in Table 2 show that, in general, both the paramagnetic shift δ^p and the spin−orbit shift δ^{SO} contribute substantially to the overall $\delta(^{195}Pt)$, while the diamagnetic shift δ^d has virtually no effect. The spin−orbit shift is typically slightly less important than the paramagnetic shift, though this varies substantially from case to case.

Origin of δ^{SO} and Its Negative Contribution to the Chemical Shift. Our calculations show that δ^{SO} (eq 7), in general adds a negative contribution to the overall chemical shift which increases in absolute terms from the lighter chlorine to the heavier iodine. The origin of this can be understood by observing that the halide ligands, with nearly degenerate lone-pair orbitals, will increasingly experience the influence of spin−orbit coupling as one descends the halogen family. When a halide-containing platinum complex is placed in a magnetic field, the spin−orbit coupling effect induces a net spin density on the halogens with a spin component opposite to the external magnetic field in order to lower the energy.[8a,19] The spin density on the halogens induces a spin density of opposite polarization on the platinum, which in turn produces an internal magnetic field opposite to the external field in the vicinity of the platinum atom. An increase in the shielding of platinum and a corresponding negative contribution to the chemical shift results.

SCHEME 1

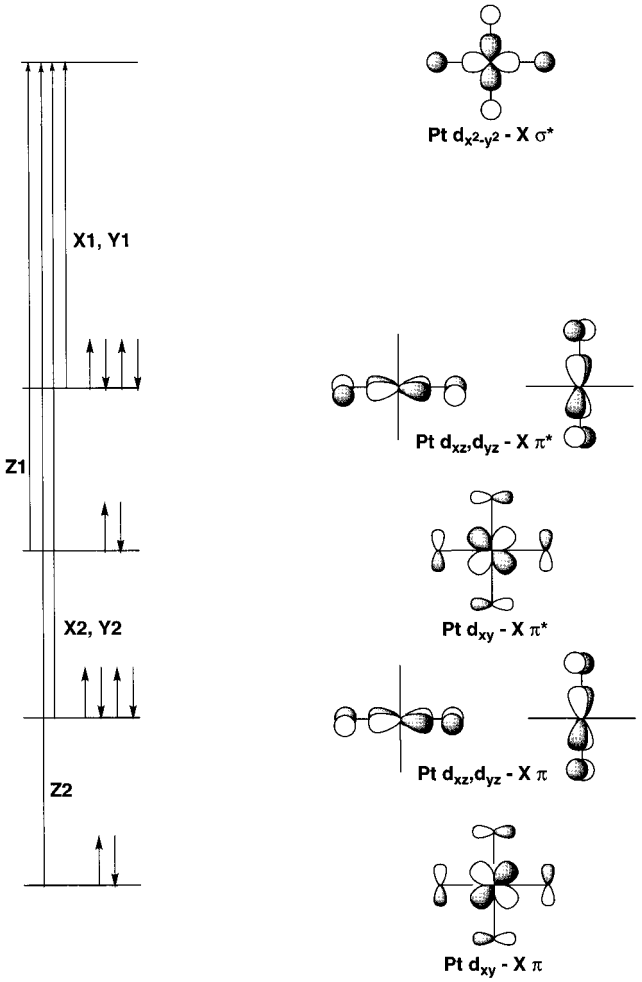

Since the spin−orbit coupling and the halide spin density increase down the halogen family, δ^{SO} correspondingly becomes more negative Cl < Br < I.

Transitions Contributing to the Paramagnetic Shielding σ^p and Shift δ^p. It is generally argued that the paramagnetic shift δ^p largely determines the overall NMR chemical shift of a heavy atom. As expressed in eqs 1−3, variances in δ^p originate from the $u^{(1)}$ coupling term of the paramagnetic shielding σ^p [represented below as $\sigma^p(u^1)$] and thus arise from two factors: the orbital energy gaps and the first-order magnetic coupling of the orbital wave functions. Our computational model allows examination of these in detail.

a. PtX_4^{2-} Anions. It is instructive to begin by examining the parent D_{4h} PtX_4^{2-} ions. The PDG eq 4 argues that the $^1A_{1g} \rightarrow {}^1A_{2g}$ transition contributes most to σ^p; in the pure d orbital case treated by the equation, this corresponds to a Pt $d_{xy} \rightarrow$ Pt $d_{x^2-y^2}$ transition. Qualitative molecular orbital theory with ligands included shows two transitions of this type, from the Pt d_{xy}−X lone pair π and Pt d_{xy}−X lone pair π^* MOs to the Pt $d_{x^2-y^2}$−X σ^* LUMO (Scheme 1, Z1 and Z2 transitions). The $^1E_g \rightarrow {}^1A_{2g}$ transition in eq 4 is a Pt $d_{xz,yz} \rightarrow$ Pt $d_{x^2-y^2}$ one; the broader MO picture sees this as a set of transitions from Pt $d_{xz,yz}$ − X lone pair π orbitals (Scheme 1, X2 and Y2 transitions) and from Pt $d_{xz,yz}$−X lone pair π^* orbitals (Scheme 1, X1 and Y1 transitions) to the Pt $d_{x^2-y^2}$−X σ^* LUMO.

Table 3 shows the results of our computational analysis of the PtX_4^{2-} ions, stemming from scalar Pauli calculations and

TABLE 3: Most Important Calculated (Scalar Pauli Method) ^{195}Pt Shielding Terms (ppm) and Corresponding Electronic Transitions, Transition Energies (eV), and Magnetic Coupling Values for PtX_4^{2-} Anions and PtL_2X_2 Compounds[e]

	transition[a]	$\sigma^p(u^1)$	$\sigma^p(u^1)_{xx}$	$\sigma^p(u^1)_{yy}$	$\sigma^p(u^1)_{zz}$	ΔE	$\langle a\|M_k\|i\rangle$	$\|\langle a\|M_k\|i\rangle\|/\Delta E_{ai}$
$PtCl_4^{2-}$	Z1	−2392	-[b]	-	−7176	2.523	0.5589	0.2215
	Z2	−948	-	-	−2845	6.372	−0.9230	0.1449
	Y1	−540	-	−1620	-	2.150	−0.2376	
	X1	−539	−1618	-	-	2.150	−0.2376	
	Y2	−388	-	−1164	-	5.257	−0.5431	
	X2	−388	−1164	-	-	5.257	−0.5431	
	total	−7836						
$PtBr_4^{2-}$	Z1	−1980	-	-	−5941	2.317	0.4743	0.2047
	Z2	−997	-	-	−2990	5.735	−0.9178	0.1600
	X1	−382	−1146	-	-	1.877	−0.1819	
	Y1	−360	-	−1080	-	1.868	−0.1764	
	X2	−359	−1076	-	-	4.581	−0.5544	
	Y2	−348	-	−1043	-	4.589	−0.5457	
	total	−7350						
PtI_4^{2-}	Z1	−1339	-	-	−4016	2.199	0.3321	0.1510
	Z2	−955	-	-	−2865	5.118	0.8833	0.1726
	Y2	−405	-	−1214	-	3.895	−0.5519	
	X2	−405	−1214	-	-	3.895	−0.5519	
	total	−5141						
cis-$Pt(NH_3)_2Cl_2$	Z1	−1357	-	-	−4069	3.160	0.4807	0.1521
	Z2	−1279	-	-	−3836	5.573	−0.8334	0.1495
	total	−7718						
trans-$Pt(NH_3)_2Cl_2$	Z2	−1460	-	-	−4372	5.638	0.9033	0.1602
	Z1	−1316	-	-	−3947	3.233	−0.5055	0.1564
	X	−1086	−3257	-	-	3.625	−0.5592	
	total	−7403						
cis-$Pt(PMe_3)_2Cl_2$	Z2	−597	-	-	−1774	6.103	0.5999	0.0983
	total	−6439						
trans-$Pt(PMe_3)_2Cl_2$	Z2	−700	-	−307	−1790	5.992		
		[−439]	[-]	[-]	[−1311]	[6.071]	[−0.6738]	[0.1110][c]
	Y2	−724	-	−539	−1633	5.740		
		[−300]	[-]	[−902]	[-]	[5.776]	[−0.5397]	[0.0934][c]
	total	−6015						
cis-$Pt(PMe_3)_2Br_2$	Z2	−713	-	-	−2139	5.833	−0.6245	0.1071
	total	−6453						
trans-$Pt(PMe_3)_2Br_2$	Z2	−915	-	−233	−2510	5.477		
		[−667]	[-]	[-]	[−2004]	[5.588]	[0.7116]	[0.1273][d]
	Y2	−783	-	−611	−1739	5.179		
		[−401]	[-]	[−1217]	[-]	[5.244]	[−0.5492]	[0.1047][d]
	total	−5859						
		[−6171]						
cis-$Pt(PMe_3)_2I_2$	Z2	−805	-	-	−2417	5.494	0.6378	0.1161
	total	−5967						
trans-$Pt(PMe_3)_2I_2$	Z2	−1067	-	−113	−3088	4.890		
		[−715]	[-]	[-]	[−2157]	[5.170]	[0.7063]	[0.1366][d]
	Y2	−761	-	−1722	−559	4.516		
		[−362]	[-]	[−1122]	[37]	[4.741]	[0.5212]	[0.1099][d]
	total	−4970						
		[−4920]						
cis-$Pt(SMe_2)_2Cl_2$	Z2	−665	-	-	−1994	5.893	0.5934	0.1007
	Z1	−594	-	-	−1794	3.088	0.2953	0.0956
	total	−6390						
trans-$Pt(SMe_2)_2Cl_2$	Z2	−926	-	-	−2777	6.404	−0.7649	0.1194
	Z1	−822	-	-	−2465	2.936	0.3476	0.1184
	total	−6265						

[a] For an orbital diagram description of the transitions, see Figure 2. [b] (−) implies $|\sigma| < 20$. [c] Scalar ZORA core values. [d] Scalar ZORA all values. [e] Values in brackets were calculated using the scalar ZORA method.

based on eq 3. One sees excellent correspondence between this analysis and that expected from eq 4. For the three halide-substituted PtX_4^{2-} anions, the two transitions contributing most to $\sigma^p(u^1)$ are the Pt d_{xy}−X lone pair $\pi \rightarrow$ Pt $d_{x^2-y^2}$−X σ^* and Pt d_{xy}−X lone pair $\pi^* \rightarrow$ Pt $d_{x^2-y^2}$−X σ^* transitions. Because the coupling of these orbitals corresponds to a rotation about the *z* axis (Scheme 2 **1a** → **2a** and **1b** → **2b**), the two contribute to $\sigma^p(u^1)_{zz}$, the *z*-directed component of the "occupied-virtual" part of the paramagnetic tensor. We therefore label them Z1 and Z2 in Scheme 1. For $PtCl_4^{2-}$, they contribute 43% of the value of $\sigma^p(u^1)$ and 39% of the overall value of σ^p. The percentages for the heavier tetrahalides are similar. The next biggest contributors to $\sigma^p(u^1)$ are transitions between the Pt d_{xz}, d_{yz}−X lone pair π and π^* combinations and the Pt $d_{x^2-y^2}$−X σ^* orbital. They correspond to rotations around *x* and *y*, contribute to $\sigma^p(u^1)_{xx}$ and $\sigma^p(u^1)_{yy}$, and are labeled X1, X2, Y1, and Y2, respectively, in Scheme 1. For $PtCl_4^{2-}$, these provide 22% of the value of $\sigma^p(u^1)$ and 20% of the value of σ^p. Thus, approximately 60% of the value of the paramagnetic shielding derives from only six transitions, with those affecting the electron density perpendicular to the unique *z* axis having the greatest effect on the magnetization, in accord with the PDG conceptualization.

The transition data provide a quantitative perspective of the relationship between the shielding and the bonding character-

SCHEME 2. PtX_4^{2-}

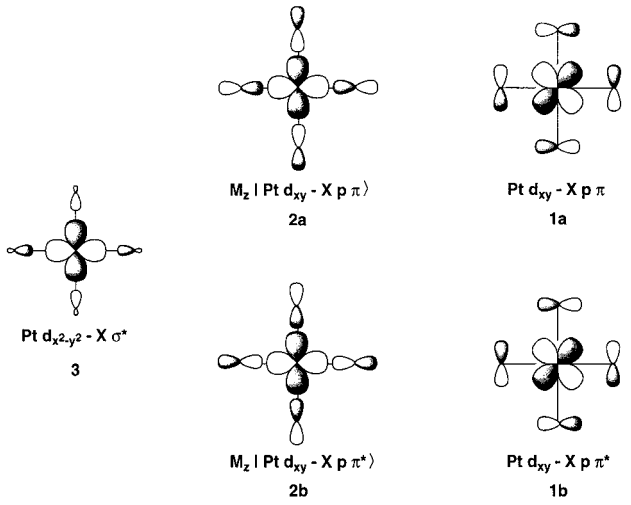

istics of the halides. Both the PDG equation and eq 3 indicate that the magnitude of $\sigma^p(u^1)$ depends on the reciprocal of the energy gap between the coupling orbitals. In the absence of other factors, one expects the magnitude of $\sigma^p(u^1)$ (and ultimately δ^p) to increase as $PtI_4^{2-} > PtBr_4^{2-} > PtCl_4^{2-}$, the reverse of the trend in crystal field splitting energy. Table 3 lists the energies of the lower energy Pt $d_{xy}-X$ lone pair $\pi^* \rightarrow$ Pt $d_{x^2-y^2}-X$ σ^* (Z1) transitions and of the higher energy Pt $d_{xy}-X$ lone pair $\pi \rightarrow$ Pt $d_{x^2-y^2}-X$ σ^* (Z2) transitions; the data confirm that the energy gaps drop down the family. However, the total $\sigma^p(u^1)$ data show that the magnitude of this term *decreases* as $PtCl_4^{2-} > PtBr_4^{2-} > PtI_4^{2-}$. The simplistic expectation is not met; another factor must reverse the trend.

The analysis points to orbital similarity as the crucial factor. Equation 3 says that $u^{(1)}$ is also determined by the first-order magnetic coupling between the occupied and virtual orbitals. This coupling is related to the similarity of the orbitals; that is, they couple better if they have similar amounts of metal and ligand atomic orbital character, worse if they have quite different amounts of metal and ligand atomic orbital character. The coupling values appear as $\langle a|M_k|i\rangle$ (shorthand for $\langle \Psi_a|\hat{M}_s|\Psi_i\rangle$, eq 3) in Table 3. For the most important transition, this term decreases down the halide family, as does the ratio $|\langle a|M_k|i\rangle|/\Delta E_{ai}$. Thus, the magnetic coupling term, not the energy gap, dictates the paramagnetic shift, and by extension much of the overall ^{195}Pt chemical shift, in PtX_4^{2-} anions.

That this coupling is greatest for chloride, smallest for iodide, implies that the Pt $d_{xy}-X$ lone pair π^* and Pt $d_{x^2-y^2}-X$ σ^* molecular orbitals are most similar for chloride, least for iodide. The model confirms this. Computationally, the Pt $d_{xy}-Cl$ lone pair π^* molecular orbital in $PtCl_4^{2-}$ contains 58% atomic Pt d_{xy} character, 41% Cl atomic p character, while the Pt $d_{x^2-y^2}-Cl$ σ^* LUMO includes 50% atomic Pt $d_{x^2-y^2}$ character, 52% Cl atomic p character.[24] In contrast, the analogous orbitals in PtI_4^{2-} are calculated as 50% Pt d, 49% I p, and 39% Pt d, 65% I p, respectively. The coupling orbitals in the tetrachloride exhibit greater AO similarity than those in the tetraiodide, so their $\langle a|M_k|i\rangle$ value is greater. This predicts the coupling trend and the shift trend correctly. Qualitatively, one can view the phenomenon as the outcome of the preference for binding of the soft iodide base rather than the harder chloride base to the soft acid Pt(II). The atomic contributions to the π^* orbitals are similar for the two halides, but the more polarizable iodide mixes in more to the σ^* LUMO, making it dissimilar to the π^* MO and lowering the magnetic coupling.

The above can be viewed similarly in terms of the PDG eq 4 and its implications of covalency. The more a ligand binds to the platinum center in a σ fashion (i.e., to the Pt $d_{x^2-y^2}$ orbital), the smaller $C^2_{A_{1g}}$ will be. The more a ligand binds to platinum in a π fashion, the smaller $C^2_{A_{2g}}$ and $C^2_{E_g}$ will be.[4] So a more covalently bound ligand will decrease σ^p, shifting the ^{195}Pt resonance downfield compared to a less covalently bound one, as long as the energy gaps do not change drastically between the two compounds. By this reasoning, the tetraiodide is more covalently bound than the tetrachloride, commensurate with HSAB theory.

Scheme 2 illustrates an important facet of the magnetic coupling. When one applies a magnetic field to a PtX_4^{2-} ion, inducing the action of the magnetization operator $\hat{M}_z$ to the Pt $d_{xy}-X$ lone pair π orbital (**2a**), the resulting "orbital" resembles the Pt $d_{x^2-y^2}-X$ σ^* orbital; the nodes are correctly aligned on both metal and ligands. Thus, a Pt $d_{xy}-X$ lone pair $\pi \rightarrow$ Pt $d_{x^2-y^2}-X$ σ^* (Z2) transition should display a sizable magnetic coupling. Table 3 bears this out: the values of $\langle a|M_k|i\rangle$ for Z2 transitions exceed any other. In contrast, application of $\hat{M}_z$ to the Pt $d_{xy}-X$ lone pair π^* orbital (**2b**) gives a resulting "orbital" with correctly aligned nodes at the metal, but incorrectly aligned nodes at the ligands, in effect, a Pt $d_{x^2-y^2}-X$ σ orbital. So a Pt $d_{xy}-X$ lone pair $\pi^* \rightarrow$ Pt $d_{x^2-y^2}$ σ^* (Z1) transition will exhibit a smaller magnetic coupling than that of the Z2 analogue above. Though not shown in the scheme, this is general for these systems: a transition emanating from a bonding orbital displays a greater magnetic coupling than that from its antibonding counterpart.

Conversely, of course, the required energy for the Z2 transition will inherently be greater than that for the Z1 transition (Scheme 1). Since the ratio of the two factors $|\langle a|M_k|i\rangle|/\Delta E_{ai}$ determines $\sigma^p(u^1)$, they compete, and which transition dominates reflects a delicate balance. For the tetrahalides, the values of $\langle a|M_k|i\rangle$ lie sufficiently close that the size of the energy gap dominates so that the Z1 transition outranks the Z2. As we shall see, this observation is not general.

b. cis- and trans-$PtX_2(NH_3)_2$. The substitution of two halides by two ammonia ligands has little impact on the transition picture. In *cis*-$PtCl_2(NH_3)_2$, the transitions contributing most to σ^p are the nominal Pt $d_{xy}-Cl$ lone pair $\pi^* \rightarrow$ Pt $d_{x^2-y^2}-X$ σ^* and Pt $d_{xy}-Cl$ lone pair $\pi \rightarrow$ Pt $d_{x^2-y^2}-X$ σ^* transitions (Table 3). These two contribute 34% of the value of $\sigma^p(u^1)$ and 32% of that of σ^p. The next four most important transitions are those from the various Pt d_{xz} and $d_{yz}-Cl$ π and π^* orbitals to the Pt $d_{x^2-y^2}-X$ σ^* orbital; they contribute 21% of the value of $\sigma^p(u^1)$, and 20% of the value of σ^p. The close correspondence between this compound and the tetrachloroplatinate anion suggests that their orbital diagrams are quite similar.

In *trans*-$PtCl_2(NH_3)_2$, the two most important transitions are still the nominal Pt $d_{xy}-Cl$ lone pair $\pi^* \rightarrow$ Pt $d_{x^2-y^2}-X$ σ^* and Pt $d_{xy}-Cl$ lone pair $\pi \rightarrow$ Pt $d_{x^2-y^2}-X$ σ^* pair; they contribute 37% of the value of $\sigma^p(u^1)$ and 35% of σ^p. Here, we see the magnetic coupling term winning over the orbital energy gap so that the Z2 transition outranks the Z1. The two contribute nearly the same to $\sigma^p(u^1)$.

Interestingly, the next most important transition, Pt $d_{yz} \rightarrow$ Pt $d_{x^2-y^2}-X$ σ^* (X),[25] contributes almost as much to $\sigma^p(u^1)$ as Z1 and Z2 do individually, a departure from prior behavior (Table 3). This holds despite the fact that, in the trans isomer, the Pt d_{yz} orbital (that in the N−Pt−N plane) is essentially nonbonding and thus dissimilar to the Pt $d_{x^2-y^2}-X$ σ^* orbital to which it couples through the magnetic operator. The middling $\langle a|M_k|i\rangle$ value results. It turns out the transition illustrates the energy

gap/magnetic coupling interplay beautifully. The competing Pt $d_{xz}-Cl$ lone pair $\pi^* \rightarrow$ Pt $d_{x^2-y^2}-X$ σ^* transition (Y1) has a smaller energy gap, but also a much smaller magnetic coupling (-0.1128), for the reason explained above and in Scheme 2. The related Pt $d_{xz}-Cl$ lone pair $\pi \rightarrow$ Pt $d_{x^2-y^2}-X$ σ^* transition (Y2) exhibits an identical magnetic coupling to X but also has a much greater ΔE (5.453 eV). The X transition contributes more to $\sigma^p(u^1)$ than the Y transitions because it combines the energy gap and magnetic coupling factors better than do the X counterparts.

Comparing the ΔE values for the Z1 transition of the cis and trans isomers to that for $PtCl_4^{2-}$ gives the well-known fact that NH_3 is a stronger crystal field splitting ligand than Cl^-. One predicts from this that $\sigma^p(u^1)$ $[PtCl_2(NH_3)_2] < \sigma^p(u^1)$ $[PtCl_4^{2-}]$, which proves true.

For PtX_2L_2 complexes containing the softer, more covalent dimethyl sulfide, trimethylphosphine, and trimethylarsine ligands, the transition picture becomes more complicated (Table 3). The percentage contribution of the most important transitions to the value of $\sigma^p(u^1)$ drops substantially. However, the pattern established above is broadly maintained. In all cases,[26] the transition contributing most to the paramagnetic shielding is the Pt $d_{xy}-X$ lone pair $\pi \rightarrow$ Pt $d_{x^2-y^2}-X$ σ^* one (Z2), providing 12−18% of the value of $\sigma^p(u^1)$. The general idea that σ^p (and by extension, the chemical shift δ) is determined most by the coupling of orbitals which affect magnetization along the molecular *z* axis holds throughout the series.

It is interesting to observe that the Z2 transitions dominate the others for these soft ligand compounds. As noted above, this reflects the magnetic coupling term outweighing the energy gap. This is somewhat unexpected, since our results for the tetrahalides clearly showed that $\langle a|M_k|i\rangle$ for the Z2 transitions decreased with increasing halide softness. One anticipates that the Z2 transition best balances the two factors, giving the largest ratio.

c. cis- and trans-$PtX_2(SMe_2)_2$. The results for the dimethyl sulfides *cis*-$PtCl_2(SMe_2)_2$ and *trans*-$PtCl_2(SMe_2)_2$ resemble those for the tetrahaloplatinates. In each case, the Z1 and Z2 transitions most determine $\sigma^p(u^1)$. Their energies roughly parallel those of the ammine analogues save that of Z2 for *trans*-$PtCl_2(SMe_2)_2$. However, the orbital coupling $\langle a|M_k|i\rangle$ is considerably smaller for the dimethyl sulfides, so consequently the ratio $|\langle a|M_k|i\rangle|/\Delta E_{ai}$ and the resulting $\sigma^p(u^1)$ are also smaller. As a result, the ^{195}Pt chemical shift of a $PtX_2(SMe_2)_2$ compound lies upfield of that of a $PtX_2(NH_3)_2$ compound.

d. cis- and trans-$PtX_2(PMe_3)_2$. By contrast, the trimethylphosphine complexes *cis*-$PtX_2(PMe_3)_2$ and *trans*-$PtX_2(PMe_3)_2$ display more complex, though consistent, behavior than the other platinum complexes. As Table 3 shows, the nominal Z1 transition becomes unimportant in determining $\sigma^p(u^1)$. The Z2 transition becomes the largest single contributor to the value of $\sigma^p(u^1)$ for *cis*-$PtCl_2(PMe_3)_2$; no other transition contributes half as much.

The two largest single contributors to the value of $\sigma^p(u^1)$ for the *trans*-bis(trimethylphosphines) are the Pt $d_{xy}-X$ lone pair $\pi^* \rightarrow$ Pt $d_{x^2-y^2}-X$ σ^* (Z2) transition and the Pt $d_{xz}-X$ lone pair $\pi \rightarrow$ Pt $d_{x^2-y^2}-X$ σ^* (Y2) one. The two appear to exhibit considerable mixing of the *yy* and *zz* components, but scalar ZORA calculations (Table 3, in brackets) demonstrate that this is an artifact of the scalar Pauli method.

The reason the Y2 transition becomes prominent in these compounds appears in Scheme 3. In trans $PtX_2(PMe_3)_2$ compounds, the Pt $d_{x^2-y^2}-X$ σ^* LUMO (**6** in the scheme) contains virtually no phosphorus character; for example, in the diiodide,

SCHEME 3. *trans*-PtX_2L_2

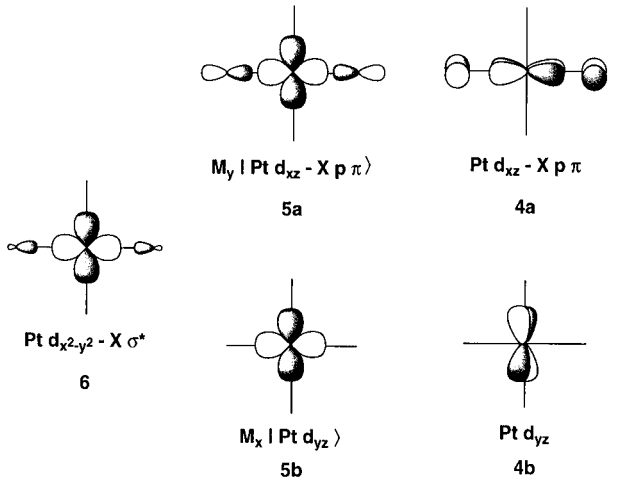

the LUMO is comprised of 43% Pt atomic orbitals, 49% Cl AOs, and ca. 2% P AOs. It will therefore couple best through the magnetic operators with molecular orbitals containing similar amounts of metal and halide character. The Pt $d_{xz}-X$ lone pair π (**4a**) and Pt $d_{xz}-X$ lone pair π^* orbitals meet this criterion, but as described above and in Scheme 2, the similarity of the former with the LUMO is greater than that of the latter (**4a** → **5a**). The Y2 transition thus contributes more to $\sigma^p(u^1)$ than the Y1. The Pt d_{yz} orbital **4b**, which takes part in the X transition, remains nonbonding, contains no halide character, and also couples less well to the LUMO (**4b** → **5b**).

Comparing this situation with that in *trans*-$PtX_2(NH_3)_2$ compounds, where the X transition proved more important that the Y types, emphasizes the subtle balances between magnetic couplings and energy gaps. In the diammines, the Y2 transition just trails the X one, while in the diphosphines the pattern reverses. While the contributions to $\sigma^p(u^1)$ differ, the X and Y transitions are always close in importance.

Comparison of the ΔE (Z2) values for the $PtCl_2(NH_3)_2$ and $PtCl_2(PMe_3)_2$ cis/trans pairs shows, unsurprisingly, that trimethylphosphine splits the metal orbitals better than does ammonia. Given this and the fact that $\langle a|M_k|i\rangle$ is smaller for the phosphine complexes than for the ammine complexes, one predicts from the equations above that δ^p for the ammines will be more positive than those for the phosphines. Table 2 shows this is so, and this readily leads to the computational result (and experimental fact) that the ^{195}Pt resonances of $PtX_2(NH_3)_2$ complexes lie at higher frequencies than those of $PtX_2(PMe_3)_2$ complexes.

The relationship between $\sigma^p(u^1)$, $\langle a|M_k|i\rangle$, and the energy gaps also explains why computationally the cis compounds are predicted to resonate at higher frequency than the trans compounds. The analysis shows that the Z2 transition for any *cis*-$PtX_2(PMe_3)_2$ species exhibits about the same $\langle a|M_k|i\rangle$ as the corresponding trans isomer, readily attributable to the identity of the ligands. However, the cis orientation of the two-electron donor ligands results in a greater orbital splitting (evaluated by ΔE) than does the trans orientation, regardless of what the halides are. This translates to a smaller $\sigma^p(u^1)$ for the cis compounds and consequently a more positive chemical shift. As it happens, this concept extends to all the compounds we surveyed; for a particular L and X, the cis and trans isomers exhibit similar magnetic couplings, with ΔE (cis) > ΔE (trans), so that δ (cis) > δ (trans) is predicted.

One can see in Table 2 that for any ligand L, as was true for the tetrahaloplatinates, the orbital energy gap (inverse of the

halide softness) varies directly with $\delta(^{195}Pt)$ rather than inversely. Table 3 shows this more quantitatively for the bis(trimethylphosphine) series. As the energy gap decreases down the family $PtCl_2(PMe_3)_2$ > $PtBr_2(PMe_3)_2$ > $PtI_2(PMe_3)_2$, the paramagnetic shielding term $\sigma^p(u^1)$ also decreases. However, the explanation we used for the PtX_4^{2-} anions proves inadequate here; the ratio $|\langle a|M_k|i\rangle|/\Delta E_{ai}$ for the Z2 transition (and for the Y2 transition of the trans isomers) *increases* down the family.

Actually, the data for the PtX_4^{2-} anions predict this behavior. One can see that the $|\langle a|M_k|i\rangle|/\Delta E_{ai}$ value for the Z2 transition increases down this family as well, contradicting the trend of the Z1 transition and the overall $\sigma^p(u^1)$. Only because the Z1 transition so dominates the value of the paramagnetic term is this irrelevant. The data in Table 3 allow rationalization of the dichotomy. If one compares the values of $\langle a|M_k|i\rangle$ for the Z1 transitions of the three tetrahalides with those for the Z2 transitions, one sees that the latter decrease more slowly than the former; the value of $\langle a|M_k|i\rangle$ for the Z2 transition of PtI_4^{2-} is 96% that of $PtCl_4^{2-}$, while the corresponding value for Z1 is 59%. Meanwhile, the ΔE values of the Z2 transition decrease far more sizably than do those for Z1. Qualitatively, one sees this as rapidly increasing stabilization of the σ^*-type Pt $d_{x^2-y^2}$ LUMO due to its decreased antibonding character down the family, while the antibonding character of the Pt d_{xy}−X π^* orbital decreases more slowly and its stabilization is less pronounced. Combination of these factors predicts that the trends of $|\langle a|M_k|i\rangle|/\Delta E_{ai}$ for the Z1 and Z2 transitions could diverge, as they do.

That $|\langle a|M_k|i\rangle|/\Delta E_{ai}$ for the Z2 transitions in *cis*- and *trans*-$PtX_2(PMe_3)_2$ compounds behaves so is thus understandable. That the overall $\sigma^p(u^1)$ decreases over the range, however, means that the less important transitions reverse the effect of the most important transitions. The trend implies that the number of transitions contributing meaningfully to $\sigma^p(u^1)$ increases from Cl > Br > I, which the analysis data bear out. For example, the sum of the next three most important contributions for cis-$PtCl_2(PMe_3)_2$ is 108% that of the first, while the corresponding number for *cis*-$PtI_2(PMe_3)_2$ is 88%. Conceptually, this means $PtCl_2(PMe_3)_2$ and $PtBr_2(PMe_3)_2$ contain more molecular orbitals which couple usefully to (and so are similar in atomic orbital makeup to) the Pt $d_{x^2-y^2}$ σ^* one than does $PtI_2(PMe_3)_2$. Evaluating this quantitatively or qualitatively is not straightforward.

Comments on the Relativistic Spin−Orbit Shift δ^{SO}. The data in Table 2 demonstrate that the contribution from δ^{SO} to the overall $\delta(^{195}Pt)$ is negative and increases considerably in absolute terms from chlorine to iodine, as discussed above. Figure 1 shows this graphically for the *cis*- and *trans*-$PtX_2(PMe_3)_2$ series. This graph underlines the necessity of including spin−orbit relativistic correction terms when predicting $\delta(^{195}Pt)$. We note that previous, more qualitative relationships such as the PDG equation have not included the influence of δ^{SO}.

A second trend in δ^{SO} is more subtle: in general, δ^{SO} (cis compounds) > δ^{SO} (trans compounds) (Table 2). Due to the ^{195}Pt NMR shift sign convention, this means trans compounds exhibit greater spin−orbit shielding σ^{SO} than do the cis analogues. The secondary trend arises because when the L ligand carries a strong trans influence, the metal−halide bond distances in cis and trans isomers differ substantially. To a first approximation, the extent to which a bonded halide atom transmits spin density (see previous discussion on the origin of δ^{SO}) to the platinum depends on the Pt−X bond distance. Since the Pt−X bond distances are typically shorter in trans compounds than in cis compounds (Table 1), we expect the behavior observed. We can confirm this simplistically with the data in Table 2 by noting that $\Delta(\delta^{SO})$ [= $|\delta^{SO}(trans) - \delta^{SO}(cis)|$] is generally smaller for PtX_2L_2 compounds where the Pt−X distances are similar for cis and trans isomers (L = NH_3, SMe_2) than when they are quite different (L = PMe_3, $AsMe_3$). In other words, when the bond distances are similar, the calculated δ^{SO} values are also similar.

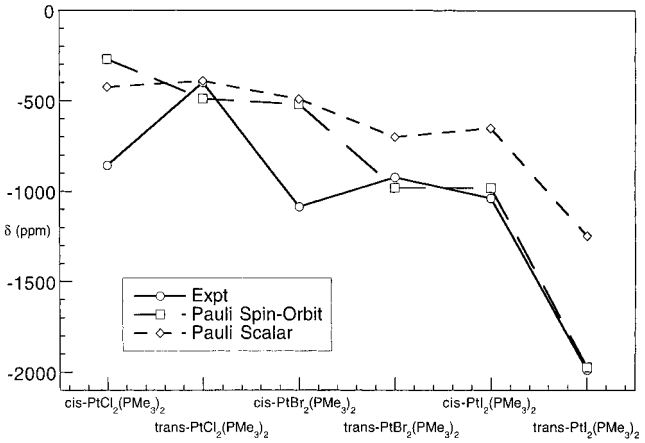

Figure 1. Plot of experimental and calculated ^{195}Pt chemical shifts for a series of $PtX_2(PMe_3)_2$. Complexes showing the need to include spin−orbit relativistic effects.

Conclusion

We have shown that density functional theory augmented with relativistic corrections predicts ^{195}Pt chemical shifts of neutral PtX_2L_2 compounds to a good degree of accuracy. Some problems yet exist, but improved models currently under study in our group will diminish them. In particular, the use of solvent models such as COSMO will expand the range of systems we can examine and will certainly give results more consistent with experiment.

The two key features of this work are the necessity of incorporating spin−orbit relativity and the considerable importance of the size of the magnetic coupling in determining the ^{195}Pt chemical shift. Both contribute to the experimental trend that platinum iodides resonate to lower frequency of platinum chlorides and to the computational trend that cis isomers resonate at lower frequencies than trans isomers. Underlying the issue of magnetic coupling is the requirement that the molecular orbitals involved be "similar", in the sense that their makeup from atomic orbitals must be similar. This feature ties in to the PDG view of covalency as a determinant of $\delta(^{195}Pt)$. When covalency is significant, i.e., when ligand−metal overlap is sizable, then the orbital similarity decreases, the magnetic coupling decreases, and the paramagnetic shift δ^p becomes more negative. The PDG equation adequately, though qualitatively, predicts the trends. The computational model predicts both the trends and the correct chemical shifts for a broader range of compounds.

Most importantly, the model improves upon the qualitative predictions in its treatment of relativistic spin−orbit coupling. While workers have recognized the importance of relativity in molecular response calculations, only recently have calculations included them explicitly. The data make clear that δ^{SO} can contribute significantly to the overall $\delta(^{195}Pt)$ and that in few cases can the platinum chemical shift be accurately predicted without including the spin−orbit shift.

Acknowledgment. T.M.G. appreciates the support of Northern Illinois University for a sabbatical during which this work was performed. This work was supported by the National Sciences and Engineering Research Council of Canada (NSERC). T.Z. acknowledges a Canada Council Killam Research Fellowship. We further thank Dr. Stephen Wolff for help and stimulating discussions.

Supporting Information Available: Graphs of δ ^{195}Pt vs Bond distances. This material is available free of charge via the Internet at http://pubs.acs.org.

References and Notes

(1) On sabbatical from the Department of Chemistry and Biochemistry, Northern Illinois University, DeKalb, IL 60115.

(2) Pregosin, P. S. *Annual Reports on NMR Spectroscopy*; Webb, G. A., Ed.; Academic Press: London, 1986; 285−349; Vol. 17.

(3) Pidcock, A.; Richards, R. E.; Venanzi, L. M. *J. Chem. Soc. A* **1968**, 1970−1973.

(4) Dean, R. R.; Green, J. C. *J. Chem. Soc. A* **1968**, 3047−3050.

(5) Goggin, P. L.; Goodfellow, R. J.; Haddock, S. R.; Taylor, B. F.; Marshall, I. R. H. *J. Chem. Soc., Dalton Trans.* **1976**, 459−467.

(6) (a) Appleton, T. G.; Hall, J. R.; Ralph, S. F. *Inorg. Chem.* **1985**, *24*, 4685−4693. (b) Appleton, T. G.; Hall, J. R.; Ralph, S. F.; Thompson, C. S. M. *Inorg. Chem.* **1989**, *28*, 1989−1993. (c) Appleton, T. G.; Bailey, A. J.; Barnham, K. J.; Hall, J. R. *Inorg. Chem.* **1992**, *31*, 3077−3082.

(7) Koie, Y.; Shinoda, S.; Saito, Y. *J. Chem. Soc., Dalton Trans.* **1981**, 1082−1088.

(8) (a) Kaupp, M.; Malkina, O. L.; Malin, V. G.; Pyykkö, P. *Chem.−Eur. J.* **1998**, *4*, 118−126. (b) Malkin, V. G.; Malkina, O. L.; Salahub, D. R. *Chem. Phys. Lett*. **1996**, *261*, 335−345.

(9) (a) Wolff, S. K.; Ziegler, T.; van Lenthe, E.; Baerends, E. J. *J. Chem. Phys.* **1999**, *110*, 7689. (b) Nakatsuji, H.; Hada, M.; Kaneko, H.; Ballard, C. C. *Chem. Phys. Lett.* **1996**, *255*, 195−202.

(10) Schreckenbach, G.; Ziegler, T. *Int. J. Quantum Chem.* **1997**, *61*, 899 and references therein.

(11) (a) Schreckenbach, G.; Ruiz-Morales, Y.; Ziegler, T. *J. Chem. Phys.* **1996**, *104*, 8605−8612. (b) Ruiz-Morales, Y.; Schreckenbach, G.; Ziegler, T. *J. Phys. Chem. A* **1997**, *101*, 4121−4127. (c) Ruiz-Morales, Y.; Ziegler, T. *J. Phys. Chem. A* **1998**, *102*, 3970−3976.

(12) (a) Rodriguez-Fortea, A.; Alemany, P.; Ziegler, T. *J. Phys. Chem. A*, submitted. (b) Hada, M.; Kaneko, H.; Nakatsuji, H. *Chem. Phys. Lett.* **1996**, *261*, 7−12.

(13) *Amsterdam Density Functional program* (ADF 2.3.3); Division of Theoretical Chemistry, Vrije Universiteit, De Boelelaan 1083, 1081 HV Amsterdam, The Netherlands; http://www.scm.com.

(14) Vosko, S. H.; Wilk, L.; Nusair, M. *Can. J. Phys.* **1980**, *58*, 1200.

(15) Perdew, J. P.; Chevary, J. A.; Vosko, S. H.; Jackson, K. A.; Pederson, M. R.; Singh, D. J.; Fiolhais, C. *Phys. Rev. B* **1992**, *46*, 6671.

(16) Snijders, J. G.; Baerends, E. J.; Ros, P. *Mol. Phys.* **1979**, *38*, 1909.

(17) van Lenthe, E. Ph.D. Dissertation, Vrije Universiteit, Amersterdam, 1996.

(18) Viewkel is part of the YAeHMOP suite of programs. Landrum, G. A. *YAeHMOP: Yet Another extended Huckel Molecular Orbital Package*. YAeHMOP is freely available on the WWW at http: overlap.chem.cornell.edu: 8080/yaehmop.html.

(19) Wolff, S. K.; Ziegler, T. *J. Chem. Phys.* **1998**, *103*, 895−905.

(20) Cambridge Crystallographic Database. Allen, F. H.; Kennard, O.; Taylor, R. *Acc. Chem. Res*. **1983**, *16*, 146−153.

(21) (a) Orpen, A. G.; Brammer, L.; Allen, F. H.; Kennard, O.; Watson, D. G.; Taylor, R. *J. Chem. Soc., Dalton Trans.* **1989**, S1−S83. (b) Allen, F. H.; Kennard, O.; Watson, D. G.; Brammer, L.; Orpen, A. G.; Taylor, R. *J. Chem. Soc., Perkin Trans. 2* **1987**, S1−S19.

(22) Ballhausen, C. J. *Introduction to Ligand Field Theory*; McGraw-Hill: New York, 1962.

(23) McGlynn, S. P.; Vanquickenborn, L. G.; Kinoshita, M.; Carroll, D. G. *Introduction to Applied Quantum Chemistry*; Hotl, Reinhart, and Winston: New York, 1972.

(24) The percentages occasionally sum to >100% due to rounding and neglect of negative contributions.

(25) Because the Pt d_{yz} orbital is nonbonding, only one transition arises from it. To indicate this unique behavior, we remove the numerical indicator.

(26) The $\sigma^{p}(u^{1})$ values determined using the scalar Pauli method indicate that the Y2 transition outranks the Z2 transition for *trans*-$PtCl_2(PMe_3)_2$. This proved artifactual; the spin−orbit Pauli calculations and the ZORA calculations reverse this order, mimicking that of the heavier halide homologues.